Ultrathin high-index metasurfaces for shaping focused beams

Mahin Naserpour,[1,2] Carlos J. Zapata-Rodríguez,[1,*] Carlos Díaz-Aviñó,[1]
Mahdieh Hashemi,[3] and Juan J. Miret[4]

[1]Department of Optics and Optometry and Vision Science, University of Valencia, Dr. Moliner 50, Burjassot 46100, Spain
[2]Department of Physics, College of Sciences, Shiraz University, Shiraz 71946-84795, Iran
[3]Department of Physics, College of Science, Fasa University, Fasa 7461781189, Iran
[4]Department of Optics, Pharmacology and Anatomy, University of Alicante, P.O. Box 99, Alicante, Spain
*Corresponding author: carlos.zapata@uv.es

The volume size of a converging wave, which plays a relevant role in image resolution, is governed by the wavelength of the radiation and the numerical aperture (NA) of the wavefront. We designed an ultrathin ($\lambda/8$ width) curved metasurface that is able to transform a focused field into a high-NA optical architecture, thus boosting the transverse and (mainly) on-axis resolution. The elements of the metasurface are metal-insulator subwavelength gratings exhibiting extreme anisotropy with ultrahigh index of refraction for TM polarization. Our results can be applied to nanolithography and optical microscopy.   © 2015 Optical Society of America

1. INTRODUCTION

The wave nature of light imposes a fundamental constraint on the attainable spatial resolution known as the diffraction limit of light [1]. Importantly, the diffraction limit has a deep impact in far-field microscopy and data storage [2,3]. According to the Rayleigh criterion, this diffraction limit is of the order of half of the wavelength for a high numerical aperture (NA). For moderate and low NAs, the transverse resolution is directly governed by the inverse of the NA of the focusing arrangement, whereas the on-axis resolution is determined by the inverse squared of its value.

Massive efforts have been carried out in order to reach and even surpass such a limit of diffraction. Gain in the spatial resolution can be achieved by introducing diffraction filters, which tune the complex-valued pattern of the converging beam in the far field, thus molding its focal distribution [4]. A plethora of alternate ways can be found in the literature, such as structuring light used in confocal (also 4Pi-confocal) scanning microscopy [5,6], by employing stimulated emission to inhibit the fluorescence process in the outer regions of the excitation point-spread function [7], two-photon excitations, and multiphoton implementations [8], to mention an few. The use of metamaterials and metasurfaces has also come on to super-resolution since they may actively control the wave direction and even transform the evanescent nature of waves into homogeneous propagating signals [9–12].

In this work, we propose an ultrathin metasurface to efficiently modify the wavefront curvature of a given converging field. In this way, we alter the focal waves by simply increasing the NA of the optical architecture. For that purpose, the beam shaping is carried out near the focal region, thus enhancing the super-resolving effect. The elements of the metasurface will be semi-transparent metal-insulator (MI) gratings with subwavelength features exhibiting an effective high index of refraction. A simple cylindrical arrangement consisting of four of these elements with incremental dephases of $\pi/2$ radians will satisfactorily serve our aim.

2. THEORY AND METHODS

Let us first consider a monochromatic converging wave field of semi-angular aperture Ω that is focused to a point F. Without loss of generality, we will consider cylindrical waves propagating in the x–z plane for which the physical problem is symmetric with respect to y axis; in addition, the magnetic field will be expressed as $\mathbf{H} = H(x, z) \exp(-i\omega t)\hat{\mathbf{y}}$, where $\hat{\mathbf{y}}$ stands for the unitary vector pointing along y axis. As illustrated in Figs. 1(a) and 1(b), we place an ultrathin metasurface, in such a way that it is concentric to the wavefront of the incident converging beam at the point F. The metasurface will reshape the cylindrical wavefront of the incident beam by increasing its curvature. At the exit of the metasurface, the field is focused to a
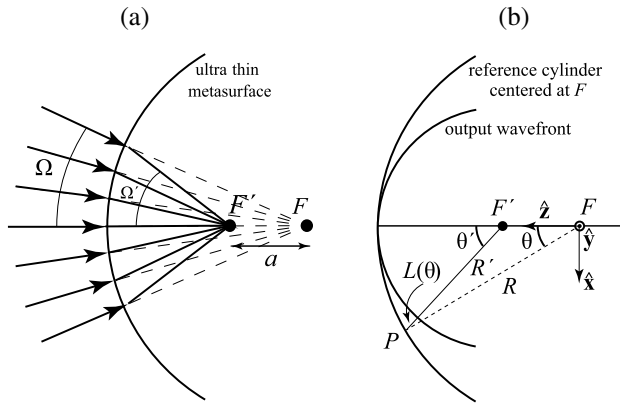
Fig. 1. (a) Geometrical interpretation of the beam shaping using optical rays. The focal point F of a given converging beam of semi-aperture angle Ω will be refocused by passing through an ultra-thin curved metasurface. (b) Schematic diagram of the converging-wave configuration and illustration of notation. The origin of the coordinate system is placed at the geometrical focus F, which is the center of the reference cylinder with radius R. The shaped emerging wave propagates in the x–z plane and deviates from the reference cylinder by $L(\theta)$.

point F' that is shifted a distance a toward this ultrathin optical element. Reshaping the wavefront of the incident converging wave leads to an increment in the NA at the exit curved surface of the metamaterial. Induced by the metasurface, the semi-angular aperture of the converging wave field is increased from Ω to Ω'. Provided that the radius of the metasurface is $R > 0$ and $a > 0$ stands for the focal shift induced by the metasurface, we infer that

$$\frac{a}{\sin(\Omega' - \Omega)} = \frac{R}{\sin(\Omega')}, \qquad (1)$$

where $\sin(\Omega')$ is the NA (in free space) of the transmitted wavefront of radius $R' = R - a$ as shown in Fig. 1(b). In Fig. 2, we present the increased NA $\sin(\Omega')$ of a given converging wavefront of NA evaluated by $\sin(\Omega)$, which is molded by a
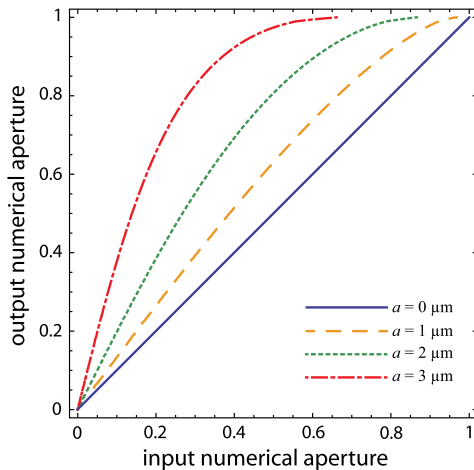

Fig. 2. Variation of the output NA, $\sin(\Omega')$, versus the input NA, $\sin(\Omega)$, for a metasurface of radius $R = 4$ µm and different values of the focal shift parameter a.

metasurface of radius $R = 4$ µm. For instance, if the incident wave field originally has an NA of 0.71 (that is, $\Omega = 45°$), then we may reach the highest emerging NA, $\sin(\Omega') = 1$, by simply shifting the focal point to a distance of $a = 2.83$ µm.

Finally, we may infer that the distance from a given point P of the reference cylinder, where the ultrathin metasurface is placed, to the wavefront of the emerging wave field of radius R', as measured along an optic ray traveling from P to F', is given by

$$L(\theta) = -(R - a) + \sqrt{R^2 + a^2 - 2aR\cos\theta}, \qquad (2)$$

where θ is the azimuthal angle as measured with respect to z axis. The optical path in excess, $L(\theta)$, must be compensated by a metasurface of amplitude transmittance

$$T(\theta) = \exp[(-ikL(\theta))], \qquad (3)$$

introducing a dephase, where $k = 2\pi/\lambda$ is the wavenumber.

According to Debye diffraction theory, the wave field in the focal region can be estimated by means of the following diffraction integral [13,14]:

$$H(\mathbf{r}) = \sqrt{\frac{kR}{2\pi i}} \exp(ikR) \int_{-\pi}^{\pi} H_s(\theta) \exp[-ik(\hat{\mathbf{q}} \cdot \mathbf{r})]d\theta, \qquad (4)$$

where the integral is evaluated over the cylindrical wavefront. In Eq. (4), $\mathbf{r} = (z, x)$ with center at focus and H_s is the scattered magnetic field as measured over the cylindrical wavefront. Finally, $\hat{\mathbf{q}} = (\cos\theta, \sin\theta)$ is a unit vector pointing from the focal point in the direction of a given point on the curved wavefront. The field amplitude, $H_s(\theta)$, which modulates the cylindrical wavefront of the converging beam, will be expressed by means of a real and positive term taking into account the truncation of the converging field.

We will consider a super-Gaussian apodization function that has the role of an aperture but minimizes edge effects and is given by

$$H_s(\theta) = H_s(0)\exp[-(\theta/\Omega)^6], \qquad (5)$$

where Ω represents the semi-aperture angle, which in addition determines the NA of the cylindrical wavefront. In Figs. 3(a)–3(c), we present the field intensity $|H(\mathbf{r})|^2$ derived from the Debye diffraction Eq. (4) for different NAs. Let us note that the field intensity is independent of the wavefront radius; however, it is clearly modified by the NA of the optical arrangement. Importantly, the intensity distribution is mirror-symmetric with respect to x and z axes, thus neglecting asymmetric spatial effects caused when the metasurface approaches the focal region [15], as we will see below. Nevertheless, Eq. (4) serves as an accurate estimation of the limit of resolution both transversally to the direction of propagation and on axis. In Fig. 3(d), we plot the full width at half-maximum (FWHM) of the central peak for different values of the wavefront NA, as measured along x and z axes. The on-axis resolution, which varies as the inverse square of the NA, is further improved than the transverse resolution, which is inversely proportional to the NA of the cylindrical wavefront.

Finally, we point out that the electric field is kept in the x–z plane for TM polarization. In high-NA arrangements, in addition, its on-axis component cannot be neglected in the focal region, resulting from applying the equation
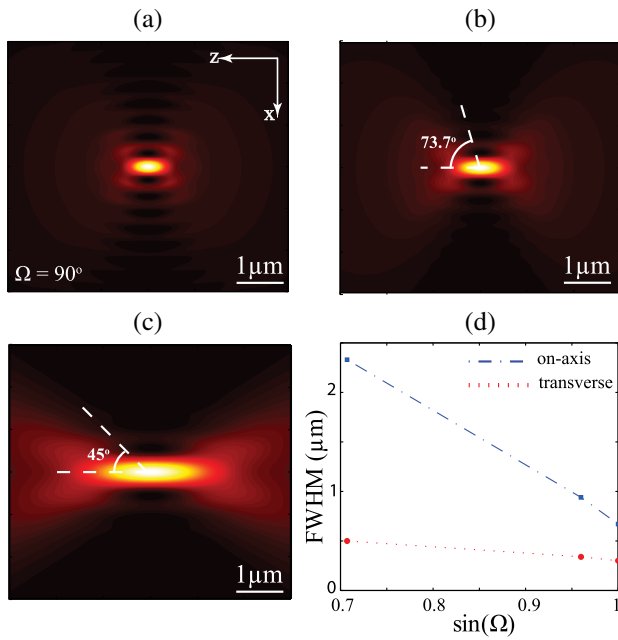
(a)   (b)

(c)   (d)

Fig. 3. Intensity pattern of the magnetic field derived from Eq. (4) at $\lambda = 800$ nm for different semi-aperture angles: (a) $\Omega = 90.0°$, (b) $\Omega = 73.7°$, and (c) $\Omega = 45.0°$. (d) FWHM of the central peak as measured along x axis (dotted line) and z axis (dashed–dotted line).

$$E_z(\mathbf{r}) = (i/\omega\epsilon_0)\partial H(x,z)/\partial x, \qquad (6)$$

where ϵ_0 is the permittivity of vacuum. The confinement of the magnetic field at the wavelength scale along the transverse direction leads to mean terms of the order of k when applying the differential operator $\partial/\partial x$. As a consequence of the vectorial nature of light, the transverse electric field E_x and the component E_z given in the previous equation can be alike in average. For axisymmetric field distributions, as we take into account here, a phase singularity of E_z will be found on axis, which may produce a deterioration of the transverse resolution [16].

3. RESULTS AND DISCUSSION

Let us demonstrate numerically that by patterning a phase distribution $\exp[(-ikL(\theta))]$ along a given converging beam, where the optical path in excess, L, is given in Eq. (2), we may produce a controlled focal shift. For that purpose, we use COMSOL Multiphysics, which is a finite-element analysis software environment for modeling and simulation of any electromagnetic system. By introducing a cylindrical surface current (SC) of radius $R = 4$ μm, which in addition is apodized by a super-Gaussian distribution with semi-aperture angle Ω, we may create a focused field around its center of curvature with an NA of 0.71 ($\Omega = 45°$), as shown in Fig. 4(a). This is in agreement with the Debye diffraction formulation, as shown in Fig. 3(c). The effect of the metasurface is simulated by including an additional phase distribution like that given in Eq. (3). In Fig. 4(b), we show the focal field of the shaped converging wave, provided that the focal shift parameter $a = 2$ μm. We observe that the molded wave field is shifted accordingly, and that the intensity distribution is essentially

that of a cylindrical converging field of a semi-angular aperture of $\Omega' = 73.7°$, as illustrated in Fig. 3(b).

The cylindrical metasurface of amplitude transmittance $T(\theta)$ can be formed by an inhomogeneous transparent material of refractive index $n(\theta) = n(0) - L(\theta)/d$, provided that d is the width of such an ultrathin layer. However, current nanotechnology presents certain limitations for the fabrication of phase-only nanoplates following a continuous variation of the refractive index n [17]. Then it is more appropriate to design a nanostructure that shapes the phase of the impinging converging field by discrete ranges. In Fig. 5, we show the result of

(a)   (b)

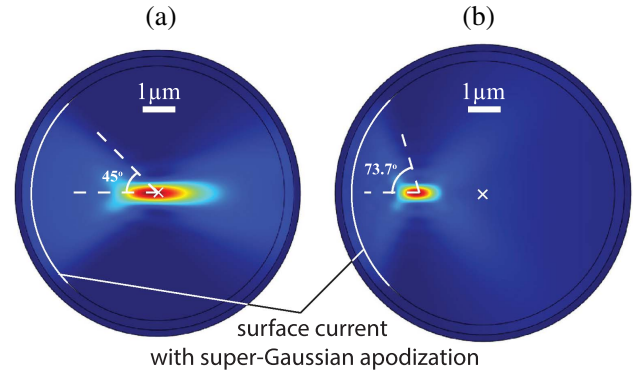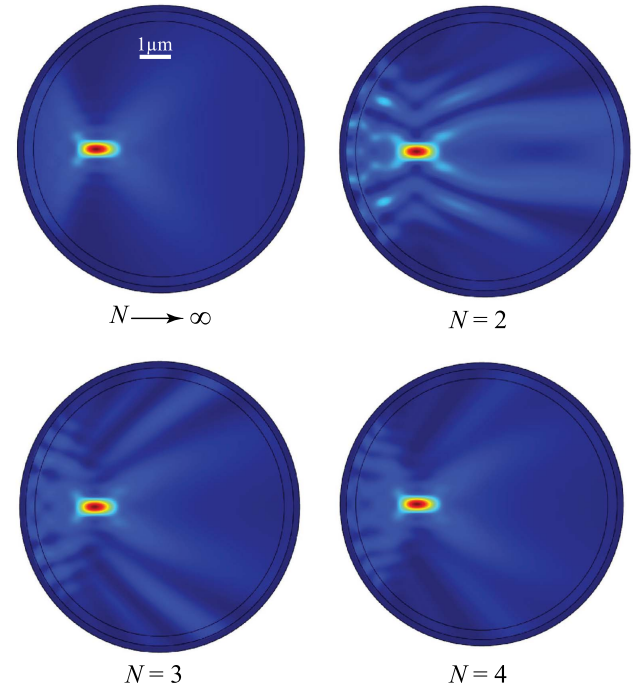surface current
with super-Gaussian apodization

Fig. 4. Intensity distribution $|H(\mathbf{r})|^2$ corresponding to a monochromatic converging wave, which is apodized at points placed at a distance $R = 4$ μm from the focus (in our model we used an SC) with (a) a super-Gaussian distribution of semi-angular aperture $\Omega = 45°$ and (b) an additional phase modulation with a prescribed parameter $a = 2$ μm. The working wavelength is $\lambda = 800$ nm. The centered white cross represents the origin of coordinates.

$N \longrightarrow \infty$ $N = 2$

$N = 3$ $N = 4$

Fig. 5. Intensity distribution $|H(\mathbf{r})|^2$ of focal waves modulated by a piecewise phase-only function $\exp[(-ikL(\theta))]$ of different number N of steps.

modulating the phase by N steps of $2\pi/N$ radians. For instance, $N = 2$ denotes a modulation of the phase in two types of zones by introducing phase shifts of π radians, leading to an effective focal shift with an increased NA, although exhibiting significant sidelobes. Provided that $N = 4$, which is carried out using four elements with different refractive indices, the resultant wave field is certainly interchangeable to the optimized design ($N \to \infty$), as illustrated in Fig. 5.

For the design of the ultrathin metasurface, where $d \ll \lambda$, we will utilize N types of (meta)materials exhibiting indices of refraction of $n_i = n_0 + i\lambda/(Nd)$, where i is an integer ranging from 0 to $N - 1$ and n_0 is an arbitrary value for the index of refraction. This procedure requires sharp tunability and a broad range of refractive indices, which has been used elsewhere [18]. An extremely high index of refraction can be obtained by using MI metamaterials, including metallic nanospheres [19] and nanolayers [20]. In our case, we consider gold nanogratings of adjustable metal filling factors $f_i = w_i/\Lambda_i$, where w_i is the width of the Au layer and Λ_i is the period of the grating (see Fig. 6). Specifically, we assume that $w_0 = 0$ so that n_0 refers to the refractive index of the bulk insulator. Assuming that propagation is carried out along the MI layers, the optical path gained by the transmitted field is $n_i d$, where

$$n_i = \mathrm{Re}\sqrt{\frac{\epsilon_d \epsilon_m}{\epsilon_d f_i + \epsilon_m(1 - f_i)}} \qquad (7)$$

is the "extraordinary" refractive index of the effective uniaxial nanostructure [21], and ϵ_m and ϵ_d are the permittivities of the metal and insulator (we chose silicon) hosting the gold nanolayers, respectively. At $\lambda = 800$ nm, we considered $\epsilon_m = -23.36 + i0.77$ for gold [22] and $\epsilon_d = 13.64$ for silicon. Assuming a discrete number of $\pi/2$ dephases ($N = 4$) and a metasurface width of $d = 100$ nm, we may infer that a sequence of $f = 0, 0.37, 0.49$, and 0.54 provides changes of two units ($n_0 = 3.69$) in the effective index of refraction, $n_i - n_{i-1} = 2$, as required.

A more accurate design may be performed by using the procedure given in Ref. [18], which is based on Floquet theory. In this case, we solved the Bloch equation for TM-polarized modes propagating with zero Bloch pseudomomentum in order to obtain the effective index for each Au-grating configuration. In Fig. 7, we show the index of refraction obtained from Eq. (7) based on the long-wavelength approximation (LWA) and that estimated from the Bloch equation for an Au–Si nanostructure assuming that the width of the silicon layer is kept fixed as
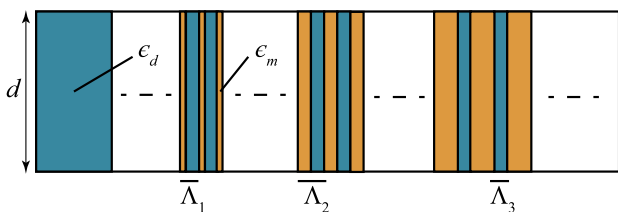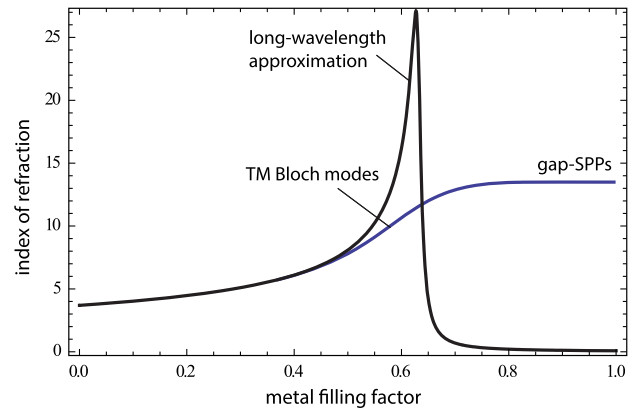

Fig. 7. Effective index of refraction of the Au–Si nanostructure based on the LWA (black solid line), that is, Eq. (7), and also evaluated by means of the Bloch equation (blue solid line) assuming that the width of the silicon layer is 15 nm.

15 nm. The Bloch approach deviates from the LWA if the widths of the Au layers reach and surpass the penetration depth of the metal [23]. The origin of this nonlocal effect in MI subwavelength gratings lies in a strong variation of the fields on the scale of a single layer [24]. In addition, homogenization of the MI nanostructure precludes the existence of gap surface plasmon polariton modes for large metal filling factors; there we may consider that the thin Si layer is sandwiched between two Au surfaces (with metal extending indefinitely on both sides of the layer) [25]. We found three periodic Au–Si compounds with prescribed effective indices of refraction, which are characterized by the following geometrical parameters: $(w_1, \Lambda_1) = (9, 24)$ nm, $(w_2, \Lambda_2) = (15, 30)$ nm, and $(w_3, \Lambda_3) = (20, 35)$ nm; again $n_0 = 3.69$ takes into account bulk silicon as a reference material. Note that the sequence of Au filling factors, $f = 0, 0.38, 0.50$, and 0.57, is in good agreement with the estimation given above based on the LWA.

Next we apply the three designed metamaterials of effective refractive indices of $n_i = n_{i-1} + 2$ (approximately, where $i = 1, 2, 3$) and silicon to arrange an ultrathin curved metasurface of 4 μm inner radius and a width of $d = 100$ nm. The assembly of Au–Si multilayers is engineered to create a phase modulation over the impinging converging wave following the function $\exp[(-ikL(\theta))]$, sampled for $N = 4$ steps, in the way we have illustrated in Fig. 5. A modulation in transmissivity also occurs due to successive reflections and refractions in the entrance and exit sides of the metasurface, and to a lesser extent due to metal losses. For instance, the modulus of the transmission factor T for pure Si gives 0.93, whereas for the subwavelength gratings it reaches 0.33, 0.61, and 0.13, set in order of increasing metal filling factor. The intensity $|H(\mathbf{r})|^2$ of the molded focal wave is calculated using COMSOL Multiphysics, as shown in Fig. 8. Apart from some nonnegligible sidelobes, we achieve a super-resolved focal spot with reduced FWHM both laterally and on axis. Specifically, the on-axis FWHM decreases to 1.2 μm, taking into account that the unshaped converging field produces a central peak with a 2.4 μm on-axis FWHM. Ultimately, we point out that in the optimal case of applying nonabsorbing materials of refractive
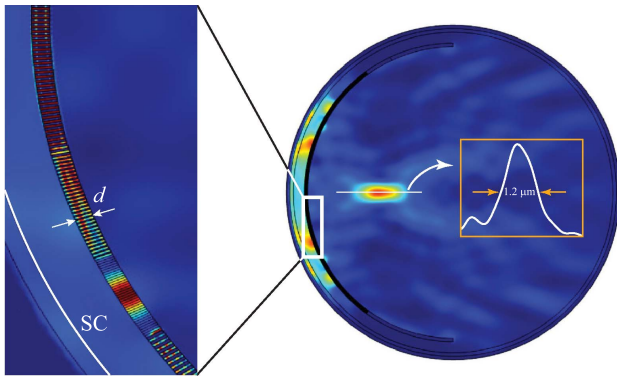

Fig. 6. Scheme of the preformed flat metasurface showing a basic arrangement of a bulk insulator and $N - 1 = 3$ metallic gratings. Neighboring elementary gratings of periods Λ_i and Λ_{i+1} will induce a dephase of $\pi/2$ radians. For the sake of clarity, we show the basic nanostructured arrangement in a planar geometry.

Fig. 8. Numerical simulation based on the finite-element method of the intensity $|H(\mathbf{r})|^2$ in the focal region of the converging field shaped by the Au–Si curved metasurface. Excitation is performed by a cylindrical SC with super-Gaussian apodization ($\Omega = 45°$), in the same way as shown in Fig. 4(a). The inset on the left shows the composition of layers in detail; the on-axis intensity in the focal region is depicted in the inset on the right.

indices n_i, an increase of 26% in the in-focus intensity is achievable.

The behavior of our curved metasurface differs substantially if the incident focused beam is transverse-electric (TE)-polarized, that is, provided the electric field may be expressed as $\mathbf{E} = E(x, z)\exp(-i\omega t)\hat{\mathbf{y}}$. Figure 9(a) shows the intensity $|E(\mathbf{r})|^2$ of the scattered field, which evidences a strong blurring of the focal spot. In this case, the wave field propagating in each metallic grating behaves like ordinary waves (o waves) in an effective uniaxial crystal of transverse (with respect to the optic axis) dielectric constant [26]

$$\epsilon_{\perp i} = f_i\epsilon_m + (1 - f_i)\epsilon_d. \tag{8}$$

Note that the circular symmetry of the nanostructure leads to an inhomogeneous distribution of the optic axis, which in addition is set perpendicular to the propagation direction of the impinging wave field. In Fig. 9(b), we represent the modal indices of TE Bloch waves propagating along the MI layers, indicating high agreement with the LWA. The modal indices in the gratings of metal widths (w_1, w_2, w_3) are (0.365, 0.087, 0.079) respectively, much lower than the refraction index of silicon. In practical terms, the phase distribution at the exit
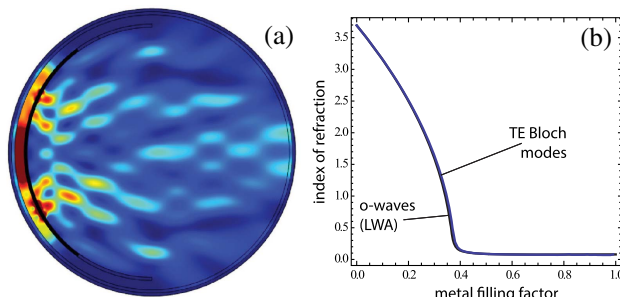

Fig. 9. (a) Intensity $|E(\mathbf{r})|^2$ of the scattered field for TE polarization. (b) Effective indices for TE-polarized waves propagating through MI lattices of different Au filling factors. The index of refraction derived from the LWA is included.
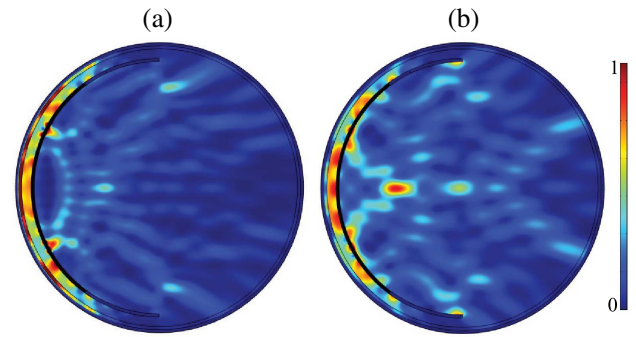

Fig. 10. Normalized intensity $|H(\mathbf{r})|^2$ in the focal region of TM-polarized converging fields of wavelengths (a) $\lambda = 700$ nm and (b) $\lambda = 900$ nm shaped by the engineered Au–Si curved metasurface.

surface is binary instead of quaternary. Moreover, increasing the metal filling factor leads to a notable decrease of the transmitted intensity, attributed to the fact that in these cases the MI lattice behaves like an opaque metal. As a result, the MI metasurface causes a serious disturbance of the complex amplitude, leading to a divergent scattered field. We point out that the examination of the polarization dependence has been carried out previously in closely related works [27].

Finally, we analyze the behavior of the engineered metasurface for TM-polarized waves with wavelengths in the vicinity of $\lambda = 800$ nm. For decreasing wavelengths, the field transmitted through the multigrating device has an averaged lower intensity, which is mainly caused by interband absorption in gold. Such reduced transmissivity is illustrated in Fig. 10(a) for $\lambda = 700$ nm where Au permittivity is set as $\epsilon_m = -15.78 + i0.66$ [22]. In these cases, metallic materials with lower loss like silver can be used, instead [28]. In addition, some spurious spots appear off axis and a ring-shaped caustic curve is evident, which are induced by a major departure from the designed phase-only term $T(\theta)$ given in Eq. (3). On the other hand, higher wavelengths reveal a more solid resistance to the rise of aberration-driven sidelobes in the focal region, as shown in Fig. 10(b) for $\lambda = 900$ nm. In the latter case, the size of the spot set at F' yields 0.99 μm on axis. It is noteworthy that the metasurface cannot fully remove the diffracted field of the incident converging field at the focal point F.

4. CONCLUSIONS

We have designed a curved metasurface for high-NA beam shaping. By using ultrahigh-refraction-index MI gratings, we have a controlled dephase of the TM-polarized transmitted wave field, modifying the curvature of the exit wavefront. The resultant increased NA demonstrates a limited gain in the transverse resolution and an exceptional super-resolution effect on axis. Finally, from a technological point of view, it is important to emphasize that the fabrication of the grating-based configuration does not present limitations since the silver and silica layer deposition by e-beam evaporation is a practicable procedure. In relation to the curved shape of the metamaterial, in addition, we point out that analogous schemes with experimental evidence have been reported elsewhere [29,30]. Our

results may be of relevance in optical microscopy and nanolithography.

REFERENCES

1. M. Born and E. Wolf, *Principles of Optics*, 7th (expanded) ed. (Cambridge University, 1999).
2. A. Toriumi, S. Kawata, and M. Gu, "Reflection confocal microscope readout system for three-dimensional photochromic optical data storage," Opt. Lett. **23**, 1924–1926 (1998).
3. C. J. R. Sheppard and A. Choudhury, "Annular pupils, radial polarization, and superresolution," Appl. Opt. **43**, 4322–4327 (2004).
4. M. Martínez-Corral, P. Andrés, C. J. Zapata-Rodríguez, and M. Kowalczyk, "Three-dimensional superresolution by annular binary filters," Opt. Commun. **165**, 267–278 (1999).
5. M. Minsky, "Memoir on inventing the confocal scanning microscope," Scanning **10**, 128–138 (1988).
6. S. Hell and E. H. K. Stelzer, "Properties of a 4Pi confocal fluorescence microscope," J. Opt. Soc. Am. A **9**, 2159–2166 (1992).
7. S. W. Hell and J. Wichmann, "Breaking the diffraction resolution limit by stimulated emission: stimulated-emission-depletion fluorescence microscopy," Opt. Lett. **19**, 780–782 (1994).
8. A. Diaspro, P. Bianchini, G. Vicidomini, M. Faretta, P. Ramoino, and C. Usai, "Multi-photon excitation microscopy," Biomed. Eng. Online **5**, 36 (2006).
9. X. Zhang and Z. Liu, "Superlenses to overcome the diffraction limit," Nat. Mater. **7**, 435–441 (2008).
10. P. Wróbel, J. Pniewski, T. J. Antosiewicz, and T. Szoplik, "Focusing radially polarized light by a concentrically corrugated silver film without a hole," Phys. Rev. Lett. **102**, 183902 (2009).
11. C. J. Zapata-Rodríguez, D. Pastor, M. T. Caballero, and J. J. Miret, "Diffraction-managed superlensing using plasmonic lattices," Opt. Commun. **285**, 3358–3362 (2012).
12. F. Aieta, P. Genevet, M. A. Kats, N. Yu, R. Blanchard, Z. Gaburro, and F. Capasso, "Aberration-free ultrathin flat lenses and axicons at telecom wavelengths based on plasmonic metasurfaces," Nano Lett. **12**, 4932–4936 (2012).
13. T. D. Visser and S. H. Wiersma, "Diffraction of converging electromagnetic waves," J. Opt. Soc. Am. A **9**, 2034–2047 (1992).
14. C. J. Zapata-Rodríguez, "Debye representation of dispersive focused waves," J. Opt. Soc. Am. A **24**, 675–686 (2007).
15. C. J. Zapata-Rodríguez, P. Andrés, M. Martínez-Corral, and L. Muñoz-Escrivá, "Gaussian imaging transformation for the paraxial Debye formulation of the focal region in a low-Fresnel-number optical system," J. Opt. Soc. Am. A **17**, 1185–1191 (2000).
16. K. S. Youngworth and T. G. Brown, "Focusing of high numerical aperture cylindrical-vector beams," Opt. Express **7**, 77–87 (2000).
17. H. Im, K. C. Bantz, N. C. Lindquist, C. L. Haynes, and S.-H. Oh, "Vertically oriented sub-10-nm plasmonic nanogap arrays," Nano Lett. **10**, 2231–2236 (2010).
18. M. Naserpour, C. J. Zapata-Rodríguez, A. Zakery, and J. J. Miret, "Highly localized accelerating beams using nano-scale metallic gratings," Opt. Commun. **334**, 79–84 (2015).
19. J. Christensen and F. J. García de Abajo, "Slow plasmonic slab waveguide as a superlens for visible light," Phys. Rev. B **82**, 161103 (2010).
20. J. T. Shen, P. B. Catrysse, and S. Fan, "Mechanism for designing metallic metamaterials with a high index of refraction," Phys. Rev. Lett. **94**, 197401 (2005).
21. P. Yeh, *Optical Waves in Layered Media* (Wiley, 1988).
22. S. Babar and J. H. Weaver, "Optical constants of Cu, Ag, and Au revisited," Appl. Opt. **54**, 477–481 (2015).
23. E. Popov and S. Enoch, "Mystery of the double limit in homogenization of finitely or perfectly conducting periodic structures," Opt. Lett. **32**, 3441–3443 (2007).
24. J. Elser, V. A. Podolskiy, I. Salakhutdinov, and I. Avrutsky, "Nonlocal effects in effective-medium response of nanolayered metamaterials," Appl. Phys. Lett. **90**, 191109 (2007).
25. S. I. Bozhevolnyi, *Plasmonic Nanoguides and Circuits* (Pan Stanford, 2009).
26. A. Yariv and P. Yeh, "Electromagnetic propagation in periodic stratified media. II. Birefringence, phase matching, and x-ray lasers," J. Opt. Soc. Am. **67**, 438–448 (1977).
27. S. Ishii, A. V. Kildishev, V. M. Shalaev, K.-P. Chen, and V. P. Drachev, "Metal nanoslit lenses with polarization-selective design," Opt. Lett. **36**, 451–453 (2011).
28. M. Naserpour, C. J. Zapata-Rodríguez, A. Zakery, C. Díaz-Aviñó, and J. J. Miret, "Accelerating wide-angle converging waves in the near field," J. Opt. **17**, 015602 (2015).
29. I. I. Smolyaninov, Y.-J. Hung, and C. C. Davis, "Magnifying superlens in the visible frequency range," Science **315**, 1699–1701 (2007).
30. J. Rho, Z. Ye, Y. Xiong, X. Yin, Z. Liu, H. Choi, G. Bartal, and X. Zhang, "Spherical hyperlens for two-dimensional sub-diffractional imaging at visible frequencies," Nat. Commun. **1**, 143 (2010).